



Design and synthesis of 4-anilinoquinazolines as Raf kinase inhibitors. Part 1. Selective B-Raf/B-Raf^{V600E} and potent EGFR/VEGFR2 inhibitory 4-(3-hydroxyanilino)-6-(1*H*-1,2,3-triazol-4-yl)quinazolines

Cheng-I Lee^{a,b}, Chu-Bin Liao^c, Chih-Shang Chen^d, Fen-Ying Cheng^d, Yu-Hsuan Chung^d, Yu-Chuan Wang^d, Sian-Yi Ciou^c, Wen-Yun Hsueh^d, Tzu-Hao Lo^d, Guan-Ru Huang^d, Hsin-Yi Huang^d, Chia-Shen Tsai^d, Yu-Jung Lu^a, Shih-Hsien Chuang^c, Jiann-Jyh Huang^{d,e,*}

^a Department of Biomedical Sciences, National Chung Cheng University, Min-Hsiung, Chia-Yi 62102, Taiwan

^b Center for Nano Bio-detections, Advanced Institute of Manufacturing with High-tech Innovations (AIM-HI), National Chung Cheng University, Min-Hsiung, Chia-Yi 62102, Taiwan

^c Development Center for Biotechnology, National Biotechnology Research Park, Taipei City 11571, Taiwan

^d Department of Applied Chemistry, National Chiayi University, No. 300, Syuefu Rd., Chiayi City 60004, Taiwan

^e The Training and Research Institute of Food and Agriculture, National Chiayi University, No. 300, Syuefu Rd., Chiayi City 60004, Taiwan

ARTICLE INFO

Keywords:

4-Anilinoquinazoline
Raf
EGFR
VEGFR
Kinase

ABSTRACT

This paper presents the design and synthesis of 4-(3-hydroxyanilino)-6-(1*H*-1,2,3-triazol-4-yl)quinazolines of scaffold **9** as selective B-Raf/B-Raf^{V600E} and potent EGFR/VEGFR2 kinase inhibitors. Total 14 compounds of scaffold **9** having different side chains at the triazolyl group with/without fluoro substituents at the anilino group were synthesized and investigated. Among them, **9m** with a 2-carbamoyl ethyl side chain and C-4'/C-6' difluoro substituents was the most potent, which selectively inhibited B-Raf (IC₅₀: 57 nM) and B-Raf^{V600E} (IC₅₀: 51 nM) over C-Raf (IC₅₀: 1.0 μM). Compound **9m** also actively inhibited EGFR (IC₅₀: 73 nM) and VEGFR2 (IC₅₀: 7.0 nM) but not EGFR^{T790M} and PDGFR-β (IC₅₀: >10 μM). Despite having good potency for B-Raf and B-Raf^{V600E} in the enzymatic assays, **9m** was less active to inhibit melanoma A375 cells which proliferate due to constitutively activated B-Raf^{V600E}. The inferior activity of **9m** for A375 was similar to that of sorafenib (**6**), suggesting that **9m** might bind to the inactive conformations of B-Raf and B-Raf^{V600E}. Docking simulations could thus be performed to reveal the binding poses of **9m** in B-Raf, B-Raf^{V600E}, and VEGFR2 kinases.

1. Introduction

Inhibition of the oncogenic protein kinases [1,2] has been proved as a successful anticancer strategy [3]. As of 1 March 2019, the U.S. FDA has approved total 43 small-molecule kinase inhibitors for the treatment of various cancers [4]. The majority of the approved kinase inhibitors is developed for receptor tyrosine kinases, among which EGFR (epidermal growth factor receptor) [5] and VEGFR (vascular endothelial growth factor receptor) [6] kinases are the best validated. Amplification or

mutation of EGFR is observed in various cancers and prevalent in non-small-cell lung cancer (NSCLC) [7]. Activation of VEGFR is responsible for tumor angiogenesis/metastasis [8,9] and correlates with the poor prognosis of cancer patients [10]. Treatment of NSCLC with EGFR inhibitors [11] as well as kidney and thyroid cancers with VEGFR inhibitors [12] are generally practiced. 4-Anilinoquinazoline (see the blue scaffold of **1–3**, Fig. 1) is a privileged structure versatile for EGFR and VEGFR inhibitions [13,14]. By introduction of distinct substituents to the anilino group, 4-anilinoquinazolines can be EGFR selective, VEGFR

Abbreviations: CuAAC, copper(I)-catalyzed alkyne–azide cycloaddition; DMF, dimethylformamide; DMSO, dimethyl sulfoxide; dppf, 1,1'-bis(diphenylphosphino)ferrocene; EGFR, epidermal growth factor receptor; ERK, extracellular-signal-regulated kinase; FDA, Food and Drug Administration; GI₅₀, the concentration for 50% of maximal inhibition of cell proliferation; H-bond, hydrogen bond; IC₅₀, the half maximal inhibitory concentration; MAPK, mitogen-activated protein kinase; MEK, mitogen-activated protein kinase kinase; NaAsc, sodium ascorbate; NSCLC, non-small-cell lung cancer; PDB, Protein Data Bank; PDGFR, platelet-derived growth factor receptor; Raf, rapid accelerated fibrosarcoma; Ras, rat sarcoma viral oncogene homolog; TBAF, tetrabutylammonium fluoride; TMSN₃, trimethylsilyl azide; VEGF, vascular endothelial growth factor; VEGFR, vascular endothelial growth factor receptor.

* Corresponding author at: Department of Applied Chemistry, National Chiayi University, No. 300, Syuefu Rd., Chiayi City 60004, Taiwan.

E-mail address: lukehuang@mail.ncyu.edu.tw (J.-J. Huang).

<https://doi.org/10.1016/j.bioorg.2021.104715>

Received 1 November 2020; Received in revised form 29 January 2021; Accepted 30 January 2021

Available online 8 February 2021

0045-2068/© 2021 Elsevier Inc. All rights reserved.

selective, or both. EGFR inhibitors gefitinib (1) [15] and lapatinib (2) [16] as well as VEGFR inhibitor vandetanib (3) [17] are the representative examples of kinase inhibitory 4-anilinoquinazolines. In addition, several modified quinazolines also show EGFR [18], VEGFR [19], and Aurora kinase [20] inhibitory activities.

Serine/threonine protein kinase Raf (rapid accelerated fibrosarcoma) [21], comprising A-Raf, B-Raf, and C-Raf, plays a central role in the Ras/Raf/MEK/ERK (MAPK, mitogen-activated protein kinase) signal transduction pathway [22]. Growth signals from cell surface receptors (e.g., EGFR and VEGFR) through this pathway to nucleus lead to cell proliferation, differentiation, and survival. Among Raf isoforms, B-Raf is more frequently mutated in cancers [23]. Constitutively activated B-Raf^{V600E} accounts for the majority of B-Raf mutations (~90%) [24] and is found in hairy cell leukemia (100%), melanoma (66%) [23], thyroid cancer (38–69%) [25,26], colorectal cancer (20%), and a variety of cancers [27]. Selective B-Raf^{V600E} inhibitors vemurafenib (4) [28] and dabrafenib (5) [29] have been approved for the treatment of advanced melanoma.

In addition to deactivating oncogenic B-Raf signaling, Raf inhibition provides an alternative way to treat the most frequently mutated (~20% in all cancers) yet elusive Ras protein [30]. C-Raf inhibitor sorafenib (6), also potently inhibiting VEGFR and PDGFR (platelet-derived growth factor receptor) families, is thus developed and approved for clinical uses [31–33]. Signals from receptor tyrosine kinases (e.g., EGFR and VEGFR) can also be blocked by the downstream Raf inhibition. On the other hand, resistance from the current B-Raf^{V600E} therapy is found associated with EGFR signaling pathway [34–36] or VEGF-A upregulation [37]. Using EGFR antibody cetuximab with drug 4 shows clinical benefits in refractory B-Raf^{V600E} metastatic colorectal cancers [38]. Combination of B-Raf^{V600E} inhibitor PLX4720 with VEGF antibody bevacizumab shows synergistic effects in vivo [39]. These findings suggested that a small-molecule Raf inhibitor with EGFR/VEGFR inhibitory activity could be useful for refractory cancers. A leading study is a new class of dual B-Raf/EGFR inhibitors reported by Ding and his colleagues [40]. The optimized compound is active to melanoma and/or colorectal cancers resistant to 4.

We surmised that a 4-anilinoquinazoline, through the introduction of proper substituents, could inhibit Raf kinases and retain its inherent activity toward EGFR and VEGFR families. Aiming at this, 4-(3-hydroxyanilino)-6-(1*H*-1,2,3-triazol-4-yl)quinazolines of scaffold 9 was rationally designed (Fig. 2). Although the structure of 9 does not resemble to those of the approved Raf inhibitors 4–6 (Fig. 1), it was a cyclic analog of azastilbene 7, a C-Raf inhibitor reported by McDonald et al. (Fig. 2) [41]. When the C-6 at the pyridinyl group of 7 was cyclized with the distal carbon of the alkene moiety (see virtual 7a, Fig. 2) and an

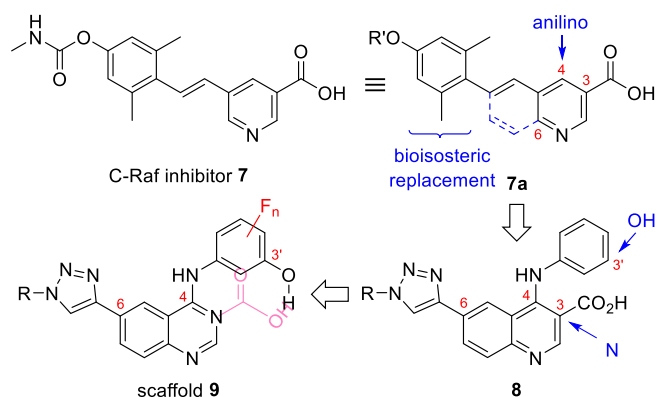


Fig. 2. Design of the Raf/EGFR/VEGFR inhibitors of scaffold 9 from C-Raf inhibitor 7 through virtual 7a and 8.

anilino group was added to the C-4 position of 7a, the 4-anilinoquinoline structure was formed in 8. The rest *o,o'*-dimethylphenyl and methylcabamoyloxy (R'O-) groups in 7a were converted to its bioisosteric triazolyl group bearing various side chains (R-) which could be readily constructed by established methods. Virtual 8 was further transformed by replacing its C-3 carboxyl group with a nitrogen atom to form the 4-anilinoquinazoline scaffold in 9, similar to the structures of EGFR and VEGFR inhibitors 1–3 (Fig. 1). As the carboxyl group is essential to the Raf inhibitory activity of 7 [41], the presence of a phenolic hydroxyl group at the C-3' position of 9 could compensate the missing carboxyl. Further addition of fluoro substituents to the anilino group could make 9 more resemble to structures of drugs 1 (4'-F) and 3 (2'-F) shown in Fig. 1, thus increasing its EGFR and VEGFR inhibitory activities. The potency of 9 toward Raf kinases might also be enhanced as the electron-withdrawing fluoro substituents could make the phenolic hydroxyl more acidic, similar to the carboxyl group in 7. Although the structure of 9 (having a C-6 triazolyl group) is similar to that of drug 2 (having a C-6 furanyl group, Fig. 1), drug 2 as well as drug 1 are reported not active to inhibit Raf kinases [42].

Herein, we reports the synthesis and optimization of scaffold 9 as our first approach to discover 4-anilinoquinazolines as Raf and EGFR/VEGFR inhibitors. We first selected proper side chains to promote the Raf inhibitory activity of 9. Subsequently, we added fluoro substituents to the anilino group of 9 to further enhance its potency toward Raf inhibition. The activity of 9 toward EGFR, VEGFR, and PDGFR was also evaluated to explore the inhibition profile of 9 and validate our design.

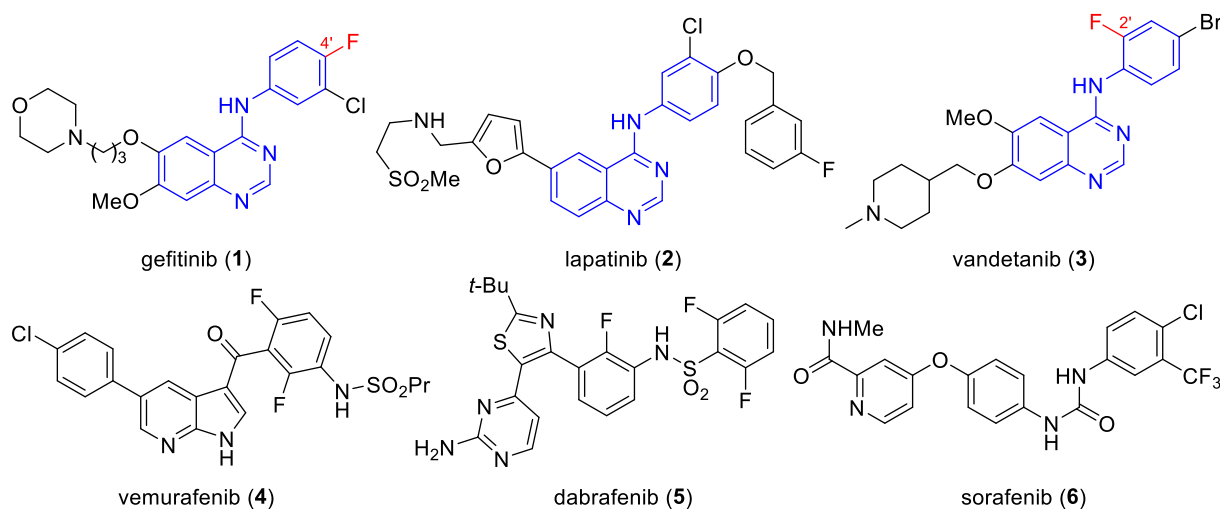


Fig. 1. Structures of FDA-approved EGFR/VEGFR inhibitory 4-anilinoquinazolines 1–3 and Raf inhibitors 4–6.

2. Results and discussion

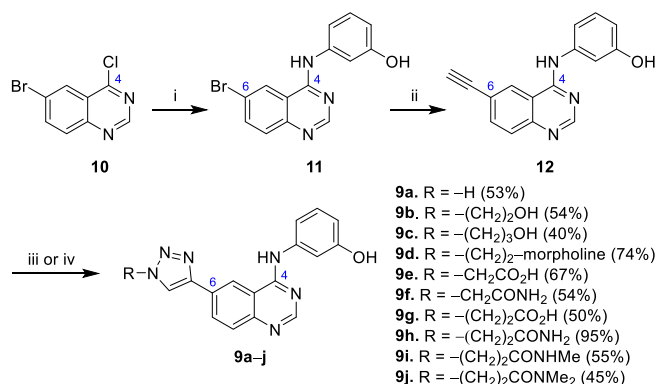
2.1. Compound synthesis

Scheme 1 presents the synthesis of 4-anilinoquinazolines **9a–j** of scaffold **9** (**Fig. 2**) bearing different side chains at the triazolyl group. 6-Bromo-4-chloroquinazoline (**10**), prepared by use of the published method [43], served as the starting material. The chloro group in **10** was substituted by 3-aminophenol to give 6-bromo-4-(3-hydroxyanilino)quinazoline (**11**) in 89% yield. Compound **11** was ethynylated by trimethylsilylacetylene using Pd(OAc)₂/CuI/dppf/Et₃N/DMF catalytic system (Sonogashira reaction) followed by desilylation with TBAF, giving 6-ethynylquinazoline **12** in 96% yield. Copper(I)-catalyzed alkyne–azide cycloaddition (CuAAC) was subsequently used to convert the C-6 ethynyl group in **12** to a triazolyl group. For the preparation of **9a** having an unsubstituted triazolyl group, **12** was cyclized with TMSN₃ by means of CuI in DMF/MeOH [44]. Compound **9a** was obtained in 53% yield. For **9b–j**, **12** was reacted with a series of alkyl azides in the CuSO₄/NaAsc/PhCO₂H catalytic system. The reaction gave the corresponding **9b–j** with a triazolyl group connected with different side chains in 40–95% yields.

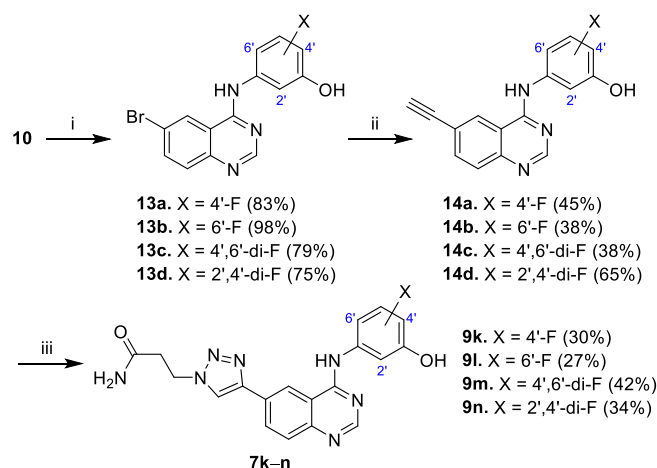
Scheme 2 illustrates the synthesis of **9k–n** bearing a fluorinated 4-anilino group and 2-carbamoyl ethyl side chain at the triazolyl moiety. Compound **10** (**Scheme 1**) served as the starting material and was reacted with a mono- or di-fluorinated 3-aminophenol. The reaction gave the corresponding **13a–d** in 75–98% yields. Compounds **13a–d** were ethynylated by trimethylsilylacetylene followed by desilylation to give the corresponding **14a–d** in 38–65% yields. Reaction of **14a–d** with 3-azidopropanamide using the CuAAC method gave the target 4-anilinoquinazolines **9k–n** having a fluoro group (**9k** and **9l**) or two fluoro groups (**9m** and **9n**) with a 2-carbamoyl ethyl side chain in 27–42% yields.

2.2. Potencies of **9a–n** of scaffold **9** to inhibit Raf and receptor tyrosine kinases

Table 1 presents the potencies of 4-(3-hydroxyanilino)-6-(1*H*-1,2,3-triazol-4-yl)quinazolines **9a–j** bearing different side chains (R) at the triazolyl group toward Raf inhibition. The potencies of clinically approved Raf inhibitors **4** and **6** as well as EGFR inhibitor **1** were also measured for comparison. Compound **9a**, having a C-6 unsubstituted triazolyl group (R = H), inhibited B-Raf and B-Raf^{V600E} at sub-micromolar concentrations (IC₅₀: 0.94 μM for B-Raf, 0.80 μM for B-Raf^{V600E}). Compound **9b**, bearing a 2-hydroxyethyl side chain, displayed increased potency (IC₅₀: 0.23 μM for B-Raf, 0.33 μM for B-



Scheme 1. Synthesis of **9a–j**. Reagents and conditions: (i) 3-aminophenol, EtOH, reflux, 89%. (ii) (a) trimethylsilylacetylene, Pd(OAc)₂, CuI, dppf, Et₃N, DMF, reflux; (b) TBAF, MeOH, 96% (two steps). (iii) For **9a**, TMSN₃, CuI, DMF, MeOH, 53%. (iv) For **9b–j**, RN₃, CuSO₄, sodium ascorbate, PhCO₂H, *t*-BuOH, H₂O, 40–95%.



Scheme 2. Synthesis of **9k–n**. Reagents and conditions: (i) fluorinated 3-aminophenol, EtOH, reflux, 75–98%. (ii) (a) trimethylsilylacetylene, Pd(OAc)₂, CuI, dppf, Et₃N, DMF, 100 °C; (b) TBAF, MeOH, 38–65% (two steps). (iii) NH₂COCH₂CH₂N₃, CuSO₄, sodium ascorbate, PhCO₂H, *t*-BuOH, H₂O, 27–42%.

Raf^{V600E}). Compound **9c**, homologous to **9b** by an extra methylene, showed slightly improved potency (IC₅₀: 0.13 μM for B-Raf, 0.24 μM for B-Raf^{V600E}). Replacement of the hydroxyl terminus at the side chain of **9b** by a morpholino group generated **9d** with decreased potency (IC₅₀: 0.98 μM for B-Raf, 0.70 μM for B-Raf^{V600E}). The carboxymethyl side chain strongly deactivated **9e** toward the two B-Raf kinases (IC₅₀: 2.2, 1.6 μM). However, replacement of the carboxyl terminus in **9e** by a carbamoyl group generated **9f** with ~3-fold enhanced potency (IC₅₀: 0.70 μM for B-Raf, 0.53 μM for B-Raf^{V600E}).

Elongation of the carboxymethyl side chain in **9e** by a methylene generated **9g** with ~8–10-fold enhanced potency (IC₅₀: 0.21 μM for both B-Raf kinases, **Table 1**). Similarly, **9h** carrying a 2-carbamoyl ethyl side chain showed significant increased potency compared to its lower homolog **9f**. Compound **9h**, respectively inhibiting B-Raf and B-Raf^{V600E} with IC₅₀ of 0.086 and 0.12 μM, was the most potent analog among the unfluorinated **9a–j**. The higher potencies of **9c**, **9g**, and **9h** implied that the hydroxyl or amino terminus at their side chains would interact with B-Raf kinases by H-bonds through a three-carbon linker. When the carbamoyl group in **9h** was mono-methylated, the resulting analog **9i** was ~4–6-times less potent (IC₅₀: 0.53, 0.48 μM) than **9h**. Compound **9j**, the dimethylated analog of **9h**, was further deactivated (IC₅₀: 1.5, 1.3 μM). As a result, the hydroxyl or amino terminus at the side chain of **9c**, **9g**, and **9h** possibly served as an H-bond donor to interact with B-Raf and B-Raf^{V600E}.

Unlike their good potencies toward B-Raf and B-Raf^{V600E}, compounds **9a–j** listed in **Table 1** were less active to inhibit C-Raf (IC₅₀: 0.52 to >10 μM). Among them, **9j** was more potent for C-Raf (IC₅₀: 0.52 μM) than B-Raf (IC₅₀: 1.5, 1.3 μM). The most potent B-Raf inhibitor **9h** merely inhibited C-Raf with an IC₅₀ of 2.8 μM, which was ~33 and ~23 less potent than inhibiting B-Raf and B-Raf^{V600E}, respectively. On the contrary, clinically used drugs **4** and **6** were very active for all the three Raf kinases with IC₅₀ of 0.0070–0.040 μM. Drug **4** was slightly more potent for B-Raf^{V600E} (IC₅₀: 0.026 μM), and drug **6** was more potent for C-Raf (IC₅₀: 0.0070 μM). The potencies for both drugs obtained in-house were similar to those from literatures [45,46]. As a result, **9h** was a more selective inhibitor for B-Raf and B-Raf^{V600E} than **4** and **6**.

We then investigated the potencies of compounds **9k–n** (**Table 2**), the fluorinated analogs of the most potent and selective B-Raf inhibitory **9h** that has a 2-carbamoyl ethyl side chain. The potencies of **9h** and **9k–n** for EGFR, EGFR^{T790M}, VEGFR2 (as a representative for VEGFR family), and PDGFR-β kinases were also determined to prove our design. For B-Raf inhibition, compound **9k**, the 4'-fluoro analog of **9h**, was less potent (IC₅₀: 0.25, 0.19 μM) than **9h** (IC₅₀: 0.086, 0.12 μM). Compound **9l**,

Table 1
Inhibitory potencies of 4-(3-hydroxyanilino)-6-(1*H*-1,2,3-triazol-4-yl)quinazolines **9a–j** toward Raf kinases.^a

9a–j

compound	R	kinase inhibitory IC ₅₀ (μM)		
		B-Raf	B-Raf ^{V600E}	C-Raf
9a	H	0.94 ± 0.05	0.80 ± 0.06	8.2 ± 1.0
9b	HO-CH ₂ -CH ₂ -CH ₂ -R	0.23 ± 0.02	0.33 ± 0.04	5.8 ± 0.3
9c^a	HO-CH ₂ -CH ₂ -CH ₂ -CH ₂ -R	0.13 ± 0.01	0.24 ± 0.03	5.3 ± 0.1
9d	HO-CH ₂ -CH ₂ -CH ₂ -N(CH ₂) ₂ -R	0.98 ± 0.14	0.70 ± 0.06	>10
9e	HO-C(=O)-CH ₂ -CH ₂ -R	2.2 ± 0.1	1.6 ± 0.2	>10
9f	H ₂ N-C(=O)-CH ₂ -CH ₂ -R	0.70 ± 0.05	0.53 ± 0.02	>10
9g	O=C-CH ₂ -CH ₂ -R	0.21 ± 0.03	0.21 ± 0.04	4.4 ± 0.3
9h	HO-C(=O)-CH ₂ -CH ₂ -R	0.086 ± 0.005	0.12 ± 0.01	2.8 ± 0.3
9i	H ₂ N-C(=O)-CH ₂ -CH ₂ -R	0.53 ± 0.04	0.48 ± 0.05	2.2 ± 0.1
9j	CH ₃ -N(CH ₃)-C(=O)-CH ₂ -CH ₂ -R	1.5 ± 0.1	1.3 ± 0.2	0.52 ± 0.06
4	–	0.038 ± 0.005	0.026 ± 0.004	0.039 ± 0.006
6	–	0.040 ± 0.003	0.029 ± 0.004	0.0070 ± 0.0005
1	–	>10	>10	>10

^a The inhibitory potency of **9c** for EGFR, EGFR^{T790M}, VEGFR2, and PDGFR-β was 3.2 ± 0.4, >10, 0.043 ± 0.005, and > 10 μM, respectively.

having a C-6' fluoro group, showed improved potency (IC₅₀: 0.14, 0.11 μM) compared to **9k** that has a C-4' fluoro group. Nevertheless, both **9k** and **9l** were less potent than **9h** for B-Raf and B-Raf^{V600E} inhibitions. For the di-fluorinated analogs, **9m** with C-4'/C-6' difluoro groups was more potent than unfluorinated **9h**, having IC₅₀ of 0.057 and 0.051 μM for B-Raf and B-Raf^{V600E}, respectively. Compound **9n** with C-2'/C-4' difluoro groups was less potent (IC₅₀: 0.18 and 0.15 μM) than **9m** and parent **9h**. Similar to **9a–i** (Table 1), **9k–n** were less active (IC₅₀: 1.0–3.7 μM) for C-Raf inhibition. Compared with drugs **4** and **6**, **9m** was ~1.5–2-fold less potent for B-Raf and B-Raf^{V600E} but far less potent for C-Raf. Similar to **9h**, **9m** was more selective for B-Raf and B-Raf^{V600E} inhibitions than **4** and **6**.

As anticipated, **9h** and **9k–n** were active for EGFR (IC₅₀: 0.073–0.42 μM) and VEGFR2 (IC₅₀: 0.0070–0.70 μM). Nevertheless, they were inactive for EGFR^{T790M} and PDGFR-β (IC₅₀: >10 μM). Compound **9m** with the best B-Raf inhibitory activity was also the most potent for EGFR (IC₅₀: 0.073 μM) and VEGFR2 (IC₅₀: 0.0070 μM). Same inhibition profile was also observed in **9c** having a 3-hydroxypropyl side chain (Table 1). However, **9m** was ~10-fold less potent compared to its structurally similar drug **1** (IC₅₀: 0.0070 μM) for EGFR inhibition. The EGFR inhibitory profile of **9m** was similar to that of **1**: they were potent for EGFR and relatively not potent for EGFR^{T790M}. On the contrary, **1** was inactive for the three Raf kinases (IC₅₀: >10 μM) and **9m** was potent for B-Raf

and B-Raf^{V600E}. For VEGFR2, **9m** was more active (IC₅₀: 0.0070 μM) than drugs **4** (IC₅₀: 0.35 μM), **6** (IC₅₀: 0.017 μM), and **1** (IC₅₀: >10 μM). As a result, we successfully added the Raf inhibitory capability to a EGFR/VEGFR inhibitory 4-anilinoquinazoline in this study. As few compounds were reported to potently inhibit Raf/EGFR/VEGFR [47,48], the lead compounds (e.g., **9h** and **9m**) from this study could be further optimized to evaluate its spectrum of anticancer activity. Adding that **9h** and **9m** was far more selective for B-Raf and B-Raf^{V600E} over C-Raf than **4** and **6**, they might be useful as a biological tool to study the cross-interactions and paradox of Raf kinases [49], especially in the field of oncology.

2.3. In vitro anticancer activity of **9m**

Nevertheless, **9m** that showed the best potency for B-Raf (IC₅₀: 57 nM) and B-Raf^{V600E} (IC₅₀: 51 nM) among the compounds listed in Table 1 and 2 was not active (GI₅₀: >10 μM, Table 3) to inhibit melanoma A375 cells that proliferate due to constitutively activated B-Raf^{V600E} (in the absence of ligands). Compounds **9a–l** and **9n** that had inferior potency to inhibit B-Raf and B-Raf^{V600E} were also not active to inhibit A375 (GI₅₀: >10 μM). Drug **6**, a type II inhibitor preferentially binding to the inactive conformation of B-Raf and B-Raf^{V600E}, was also found less active for A375 (GI₅₀: 6.3 μM). In contrast, the type I inhibitor

Table 2Inhibitory potencies of 4-(3-hydroxyanilino)-6-(1*H*-1,2,3-triazol-4-yl)quinazolines **9h** and **9k–n** toward Raf, EGFR, EGFR^{T790M}, VEGFR2, and PDGFR- β kinases.^a

9h and 9k–n

compound	Ar	kinase inhibitory IC ₅₀ (μM)						
		B-Raf	B-Raf ^{V600E}	C-Raf	EGFR	EGFR ^{T790M}	VEGFR2	PDGFR- β
9h		0.086 ± 0.005	0.12 ± 0.01	2.8 ± 0.3	0.18 ± 0.04	>10	0.070 ± 0.009	>10
9k		0.25 ± 0.02	0.19 ± 0.02	3.7 ± 0.4	0.18 ± 0.03	>10	0.064 ± 0.005	>10
9l		0.14 ± 0.02	0.11 ± 0.02	2.3 ± 0.2	0.14 ± 0.02	>10	0.012 ± 0.001	>10
9m		0.057 ± 0.004	0.051 ± 0.003	1.0 ± 0.1	0.073 ± 0.004	>10	0.0070 ± 0.0005	>10
9n		0.18 ± 0.01	0.15 ± 0.02	2.8 ± 0.2	0.42 ± 0.03	>10	0.70 ± 0.05	>10
4	–	0.038 ± 0.005	0.026 ± 0.004	0.039 ± 0.006	>1.0	>1.0	0.35 ± 0.02	2.3 ± 0.3
6	–	0.039 ± 0.003	0.032 ± 0.004	0.0090 ± 0.0005	>10	>10	0.017 ± 0.002	0.065 ± 0.008
1	–	>10	>10	>10	0.0070 ± 0.0005	0.46 ± 0.03	3.3 ± 0.1	>10

Table 3In vitro anticancer activity of **9m**, **9h**, **6**, **4**, and **1**.

compound	anticancer GI ₅₀ (μM)			
	A375	PC-9	HCC827	H1975
9m	>10	6.0 ± 0.2	1.3 ± 0.3	>10
9h	>10	6.4 ± 0.6	3.2 ± 0.2	>10
6	6.3 ± 0.4	>10	>10	>10
4	0.19 ± 0.02	>10	>10	>10
1	>10	0.053 ± 0.006	0.043 ± 0.002	>10

4 which binds to the active conformation of B-Raf^{V600E}, inhibited A375 potently (IC₅₀: 0.19 μM). As a result, **9m** might act on the inactive conformations of B-Raf and B-Raf^{V600E} as **6** does. The lower enzymatic activity of **9m** than **6** for B-Raf and B-Raf^{V600E} (~1.5-fold less potent)

could further deactivate its cell activity. Another possibility for the inactivity of **9m** was that the activity of C-Raf might also contribute the proliferation of A375. Although **9m** was active for B-Raf and B-Raf^{V600E}, its low potency for C-Raf (IC₅₀: 1.0 μM) retarded its cell activity. Finally, **9m** might not have good cell permeability, thus reducing its cell activity. Drug **1** without Raf inhibitory activity (IC₅₀: >10 μM, Table 2) was inactive for A375 proliferation.

For 1-sensitive/EGFR-mutant NSCLC cells PC-9 and HCC827, **9m** only showed moderate potency (GI₅₀: 6.0 μM for PC-9, 1.3 μM for HCC827, Table 3). This would result from ~10 times inferior enzymatic EGFR inhibitory activity of **9m** (IC₅₀: 0.073 μM) relative to that of **1** (IC₅₀: 0.0070 μM). Also, the cell permeability would affect the activity of **9m** in cell. Both **9m** and **1** were inactive to NSCLC H1975 cells that harbor EGFR^{L858R/T790M} mutation (GI₅₀: >10 μM). This should

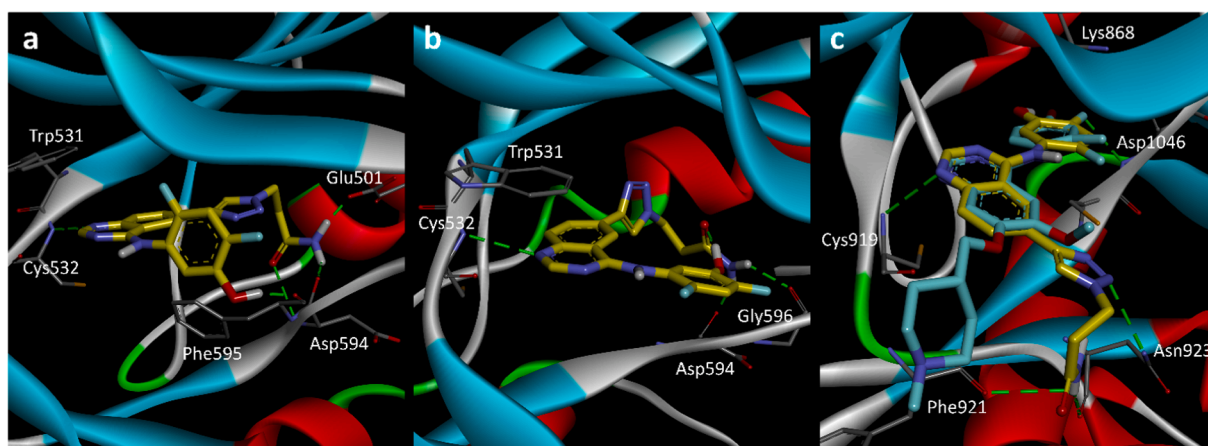


Fig. 3. Docking simulations of **9m** in the kinase domains of B-Raf, B-Raf^{V600E}, and VEGFR2. (a) Compound **9m** in B-Raf (PDB entry 1UWH). (b) Compound **9m** in B-Raf^{V600E} (PDB entry 1UWJ). (c) Overlapping of the binding poses of **9m** and drug **3** in VEGFR2 (4AGD). Compounds **9m** and **3** are shown in yellow and light blue sticks, respectively; H-bonds are shown as dashed green line; and the nitrogen, oxygen, and fluorine atoms are colored blue, red, and light blue, respectively. (For interpretation of the references to colour in this figure legend, the reader is referred to the web version of this article.)

Table 4

Calculated binding energy of **9m** in B-Raf and B-Raf^{V600E} with inactive or active conformation.

PDB entry	B-Raf	conformation	calculate binding energy (Kcal/mol)
1UWH	wt	inactive	-10.35
4KSP	wt	inactive	-10.30
1UWJ	V600E	inactive	-9.79
4G9R	V600E	inactive	-9.88
3C4C	wt	active	-8.68
4MNE	wt	active	-7.24
3OG7	V600E	active	-8.53
4XV2	V600E	active	-8.25

result from the low potency of **9m** (IC₅₀: >10 μM) and **1** (IC₅₀: 0.46 μM) for EGFR^{T790M}. Similar anticancer profile was also observed in unfluorinated **9h** to inhibit PC-9 (GI₅₀: 6.4 μM), HCC827 (GI₅₀: 3.2 μM), and H1975 (GI₅₀: >10 μM). Compound **9c** (Table 1), less active for EGFR (IC₅₀: 3.2 μM) and EGFR^{T790M} (IC₅₀: >10 μM), was not active to inhibit PC-9, HCC827, and H1975 (GI₅₀: >10 μM). Similarly, Raf inhibitors **4** and **6** did not inhibit the proliferation of the three cancer cells (GI₅₀: >10 μM) as they were inactive for EGFR and EGFR^{T790M} (IC₅₀: >1.0 μM, Table 2). Cumulatively, compound **9m** showed its anticancer activity in PC-9 and HCC827 cells through EGFR inhibition.

2.4. Interaction of **9m** with B-Raf, B-Raf^{V600E}, and VEGFR2

To explore the interaction of scaffold **9** with B-Raf kinases, we docked the most potent **9m** into the kinase domains of B-Raf (PDB entry 1UWH) [50] and B-Raf^{V600E} (PDB entry 1UWJ) [50] both having the inactive DFG-out conformations using Autodock [51] software. In B-Raf (Fig. 3a), **9m** was found to occupy the ATP-binding pocket by forming an H-bond with the hinge residue Cys532 through its quinazoline N-1 atom and stacked with Trp531 through its bicyclic π system. The phenolic hydroxyl group in **9m** served as an H-bond donor to interact with Phe595 in the DFG motif. The carbamoyl terminus at the side chain of **9m** formed two H-bonds with Asp594 in the DFG motif and one H-bond with Glu501. In B-Raf^{V600E} (Fig. 3b), **9m** also formed an H-bond with Cys532 and stacked with Trp531 in the ATP-binding pocket. An intramolecular H-bond formed between the phenolic hydroxyl and the carbonyl of the carbamoyl of **9m**, which assisted the NH₂ terminus donating two H-bonds to Asp594 and Gly596 in the DGF motif. The multiple H-bond interaction of **9m** with B-Raf and B-Raf^{V600E} should be important for its enzymatic activity as the secondary amide **9i** and tertiary amide **9j** were less active than primary amide **9h** (Table 1).

Compound **9m** was also docked into a series of B-Raf and B-Raf^{V600E} crystal structures with inactive DFG-out or active DFG-in conformation by Autodock. The calculated binding energy of the most stable pose of **9m** in these crystals was shown in Table 4. Compound **9m** was found to have stronger interactions with DFG-out B-Raf (1UWH and 4KSP) and B-Raf^{V600E} (1UWJ and 4G9R) with binding energy of -9.79 to -10.35 Kcal/mol. The interaction of **9m** with DFG-in B-Raf (3C4C and 4MNE) and B-Raf^{V600E} (3OG7 and 4XV2) was weaker (-7.24 to -8.68 Kcal/mol). The difference in binding energy (~1–2 Kcal/mol) supported the preference of **9m** to interact with B-Raf and B-Raf^{V600E} having inactive DFG-out conformations. Furthermore, the interaction of **9n** with B-Raf and B-Raf^{V600E} was also explored by docking simulations to account for its inferior potency than that of its isomeric **9m** (Supplementary Fig. S1).

The triazolyl group at the C-6 position of **9** was originally designed to imitate the phenyl group of azastilbene **7** as it can be readily constructed by the well-established Sonogashira and CuACC reactions (Fig. 2). However, results from docking simulations revealed that the triazolyl group only interacted with the alkyl groups of the proximal residues in B-Raf and B-Raf^{V600E} through its π system (π-alkyl interactions). The three nitrogen atoms of the triazolyl group did not form energy-favored bonds (e.g., H-bond) with B-Raf and B-Raf^{V600E} (Fig. 3a and 3b). The

triazolyl group could thus be replaced with other substituents. In our other study [43], we had synthesized and evaluated a series of C-6 phenyl analogs of **9** with more diverse substituents at the 4-anilino group. Results from that study suggested that the C-3' hydroxyl group was essential for the Raf inhibitory potency of **9** as the C-3' methoxy analog showed >10-fold decreased potency. Fluoro substituent at the 4-anilino group also improved the potency while chloro substituent did not. On the contrary, electron-donating methyl or methoxy group reduced the Raf inhibitory potency significantly. Some of C-6 phenyl analogs of **9** in that study [43] was more active than **9m** to inhibit Raf and EGFR kinases and thus inhibited the proliferation of A375 (GI₅₀: <1.0 μM) and PC-9 (GI₅₀: <0.2 μM) more potently.

The interaction of **9m** with VEGFR2 (PDB entry 4ADG) [52] was also explored by docking simulation as **9m** actively inhibited VEGFR2 at low nanomolar concentrations (IC₅₀: 7.0 nM, Table 2) and was more potent than drug **6** (IC₅₀: 17 nM). The binding pose of **9m** in VEGFR2 is overlapped with that of 4-anilinoquinazoline drug **3** and shown in Fig. 3c. The 4-anilinoquinazoline scaffolds of **9m** and **3** aligned well in the kinase domain of VEGFR2, both occupying the ATP-binding cleft by their quinazoliny moiety and forming an H-bond with the hinge residue Cys919. The anilino groups of **9m** and **3** buried in the back pocket of VEGFR2 and contacted with Lys868 through a π-cation interaction. The phenolic hydroxyl of **9m** formed an additional H-bond with Asp1046 than **3** in the back pocket. On the other hand, the C-6 side chain of **9m** and the C-7 side chain of drug **3** headed to the different regions in VEGFR2. The carbamoyl terminus of **9m** formed two H-bonds with Phe921 and Asn923, and the triazolyl group formed one H-bond with Asn923. These H-bond interactions could account for the high potency of **9m** for VEGFR2 inhibition.

3. Conclusions

We have developed 4-(3-hydroxyanilino)-6-(1*H*-1,2,3-triazol-4-yl) quinazolines of scaffold **9** as selective B-Raf/B-Raf^{V600E} and potent EGFR/VEGFR2 kinase inhibitors. For Raf kinases, the most potent and selective **9m** inhibited B-Raf/B-Raf^{V600E} at low nanomolar concentrations (IC₅₀: 57 and 50 nM) and was less potent toward C-Raf (IC₅₀: 1.0 μM). For receptor tyrosine kinases, **9m** was potent for EGFR (IC₅₀: 73 nM) and VEGFR2 (IC₅₀: 7.0 nM) but inactive (IC₅₀: >10 μM) for EGFR^{T790M} and PDGFR-β. Compound **9m** inhibited cell proliferation attributed to EGFR inhibition. Docking simulations were performed to analyze the binding poses of **9m** in B-Raf, B-Raf^{V600E}, and VEGFR2.

4. Experimental section

4.1. Compound synthesis

Merck Reagents Silica Gel 60 (particle size of 0.063–0.200 mm, 70–230 mesh ASTM) was used for column chromatography. Melting points were measured on STUARTTM SMP3 melting point apparatus. ¹H (400 MHz) and ¹³C (100 MHz) NMR spectra were recorded on Agilent 400-MR spectrometer using DMSO-*d*₆ as the solvent. High-resolution mass spectra were measured on LTQ Orbitrap XL mass spectrometer (Thermo Fisher Scientific). The purities of the compounds for biological evaluations (>95%) were determined from an Agilent 1100 series HPLC equipped with Agilent ZORBAX SB-C18 column (5 μm, 4.6 mm × 150 mm) and a UV detector (254 nm) using gradient of 35–100% CH₃CN in H₂O for 20 min and 100% CH₃CN for 10 min.

4.1.1. Standard procedure for the synthesis of 4-(3-hydroxyanilino)-6-bromoquinazolines **11** and **13a–d**

6-Bromo-4-chloroquinazoline (**10**, ~5.0 g, 1.0 equiv) and the corresponding 3-aminophenol (1.5 equiv) were mixed in EtOH (25 mL). The reaction mixture was heated under reflux for 12 h. The solution was cooled to room temperature and the resulting precipitate was collected by filtration. The solids were washed with EtOH (20 mL) and air-dried to

give the targets **11** and **13a–d** as solids in 75–98% yields.

4.1.1.1. 3-[(6-Bromoquinazolin-4-yl)amino]phenol (11). Yield: 89%; mp 233.1–234.8 °C; ¹H NMR: δ 11.10 (brs, 1H), 9.72 (brs, 1H), 9.07 (s, 1H), 8.88 (s, 1H), 8.19 (d, *J* = 8.8 Hz, 1H), 7.83 (d, *J* = 8.8 Hz, 1H), 7.28–7.12 (m, 3H), 6.71 (d, *J* = 7.7 Hz, 1H); ¹³C NMR: δ 157.8, 157.5, 152.9, 138.5, 137.5, 129.3, 126.4, 125.7, 119.9, 115.7, 114.2, 112.6, 110.6, 109.5; HRMS calcd for [C₁₄H₁₀BrN₃O + H]⁺ 316.0080, found 316.0101.

4.1.1.2. 5-[(6-Bromoquinazolin-4-yl)amino]-2-fluorophenol (13a). Yield: 83%; mp 279.6–280.9 °C; ¹H NMR: δ 11.47 (s, 1H), 10.28 (s, 1H), 9.15 (s, 1H), 8.91 (s, 1H), 8.22 (d, *J* = 8.9 Hz, 1H), 7.89 (d, *J* = 8.9 Hz, 1H), 7.38 (dd, *J* = 8.0, 2.5 Hz, 1H), 7.24 (dd, *J* = 11.0, 8.8 Hz, 1H), 7.15–7.10 (m, 1H); ¹³C NMR: δ 159.4, 158.7, 151.0, 149.5 (d, *J* = 241.6 Hz), 144.9 (d, *J* = 13.0 Hz), 138.8, 137.6, 132.6 (d, *J* = 2.8 Hz), 127.4, 121.0, 115.9 (d, *J* = 5.1 Hz), 115.7 (d, *J* = 7.6 Hz), 114.9, 114.5 (d, *J* = 2.7 Hz); HRMS calcd for [C₁₄H₉BrFN₃O + H]⁺ 333.9986, found 334.0013.

4.1.1.3. 3-[(6-Bromoquinazolin-4-yl)amino]-4-fluorophenol (13b). Yield: 98%; mp 282.9–284.2 °C; ¹H NMR: δ 11.64 (s, 1H), 9.81 (s, 1H), 9.11 (s, 1H), 8.90 (s, 1H), 8.24 (d, *J* = 9.0 Hz, 1H), 7.90 (d, *J* = 9.0 Hz, 1H), 7.18 (t, *J* = 9.4 Hz, 1H), 6.94–6.89 (m, 1H), 6.83–6.77 (m, 1H); ¹³C NMR: δ 160.2, 154.2 (d, *J* = 1.6 Hz), 151.7, 150.4 (d, *J* = 239.4 Hz), 139.5, 138.4, 127.9, 124.3 (d, *J* = 14.2 Hz), 122.5, 121.6, 116.9 (d, *J* = 21.2 Hz), 116.0 (d, *J* = 7.1 Hz), 115.0, 114.8; HRMS calcd for [C₁₄H₉BrFN₃O + H]⁺ 333.9986, found 334.0011.

4.1.1.4. 5-[(6-Bromoquinazolin-4-yl)amino]-2,4-difluorophenol (13c). Yield: 79%; mp 225.1–226.9 °C; ¹H NMR: δ 11.60 (brs, 1H), 10.29 (brs, 1H), 9.08 (s, 1H), 8.90 (s, 1H), 8.24 (d, *J* = 8.9 Hz, 1H), 7.89 (d, *J* = 8.9 Hz, 1H), 7.42 (t, *J* = 9.4 Hz, 1H), 7.13 (t, *J* = 8.3 Hz, 1H); ¹³C NMR: δ 160.3, 151.8, 150.0 (dd, *J* = 245.1, 10.9 Hz), 149.3 (dd, *J* = 242.4, 10.7 Hz), 142.0 (dd, *J* = 12.7, 2.6 Hz), 139.5, 138.5, 127.9, 122.6, 121.6, 119.9 (dd, *J* = 13.9, 3.6 Hz), 116.6 (d, *J* = 2.8 Hz), 115.0, 105.6 (t, *J* = 24.4 Hz); HRMS calcd for [C₁₄H₈BrF₂N₃O + H]⁺ 351.9892, found 351.9881.

4.1.1.5. 3-[(6-Bromoquinazolin-4-yl)amino]-2,6-difluorophenol (13d). Yield: 75%; mp 299.0–300.8 °C; ¹H NMR: δ 12.00 (s, 1H), 10.52 (s, 1H), 9.25 (s, 1H), 8.91 (s, 1H), 8.24 (d, *J* = 8.9 Hz, 1H), 7.97 (d, *J* = 8.9 Hz, 1H), 7.14 (t, *J* = 9.5 Hz, 1H), 6.98–6.90 (m, 1H); ¹³C NMR: δ 160.3, 152.1 (dd, *J* = 242.3, 5.3 Hz), 151.9, 148.2 (dd, *J* = 246.5, 6.7 Hz), 139.5, 138.8, 135.0 (dd, *J* = 16.8, 14.7 Hz), 127.9, 122.8, 121.5, 121.4 (d, *J* = 3.1 Hz), 117.4 (d, *J* = 8.5 Hz), 115.1, 111.6 (dd, *J* = 19.8, 3.1 Hz); HRMS calcd for [C₁₄H₈BrF₂N₃O + H]⁺ 351.9892, found 351.9912.

4.1.2. Standard procedure for the synthesis of 6-ethynyl-4-(3-hydroxyanilino)quinazolines 12 and 14a–d

Compound **11** or **13a–d** (~10.0 mmol, 1.0 equiv) was mixed with CuI (0.10 equiv), Pd(OAc)₂ (0.010 equiv), and 1,1'-bis(diphenylphosphino)ferrocene (dppf, 0.060 equiv) in anhydrous DMF (50 mL). The solution was added with Et₃N (10 mL) and trimethylsilylacetylene (10 equiv). After purged with nitrogen to remove oxygen, the reaction mixture was heated under reflux for 12 h. The solution was cooled to room temperature, added with EtOAc, and stirred for 30 min. The solution was passed through a short column packed with silica gel, and the filtrate was washed with water and aqueous NH₄Cl. The organic layer was collected, dried over anhydrous MgSO₄, and concentrated under reduced pressure. The residue was re-dissolved in MeOH, added with TBAF (3.0 equiv), and stirred at room temperature for 60 min under N₂. The solution was concentrated under reduced pressure to remove most solvent. The residue was added with water and stirred for 10 min. The resulting solids were collected by filtration to give the targets **12** or

14a–d as solids in 38–96% yields.

4.1.2.1. 3-[(6-Ethynylquinazolin-4-yl)amino]phenol (12). Yield: 96%; mp 148.9–150.5 °C; ¹H NMR: δ 9.75 (s, 1H), 9.44 (s, 1H), 8.80 (d, *J* = 1.4 Hz, 1H), 8.60 (s, 1H), 7.85 (dd, *J* = 8.6, 1.4 Hz, 1H), 7.74 (d, *J* = 8.6 Hz, 1H), 7.41 (t, *J* = 2.0 Hz, 1H), 7.26 (d, *J* = 7.8 Hz, 1H), 7.15 (t, *J* = 7.8 Hz, 1H), 6.54 (dd, *J* = 7.8, 2.0 Hz, 1H), 4.39 (s, 1H); ¹³C NMR: δ 157.9, 157.6, 155.8, 149.9, 140.4, 135.7, 129.5, 128.7, 127.4, 119.7, 115.5, 113.5, 111.5, 109.9, 83.5, 82.3; HRMS calcd for [C₁₆H₁₁N₃O + H]⁺ 262.0975, found 262.1001.

4.1.2.2. 5-[(6-Ethynylquinazolin-4-yl)amino]-2-fluorophenol (14a). Yield: 45%; mp 296.1–298.2 °C; ¹H NMR: δ 9.95 (s, 1H), 9.79 (s, 1H), 8.76 (s, 1H), 8.57 (s, 1H), 7.85 (d, *J* = 8.5 Hz, 1H), 7.74 (d, *J* = 8.5 Hz, 1H), 7.57 (dd, *J* = 8.2, 2.4 Hz, 1H), 7.24–7.19 (m, 1H), 7.13 (dd, *J* = 11.0, 8.9 Hz, 1H), 4.41 (s, 1H); ¹³C NMR: δ 157.6, 155.8, 149.9, 148.2 (d, *J* = 238.0 Hz), 144.9 (d, *J* = 12.9 Hz), 135.7, 135.7 (d, *J* = 2.7 Hz), 128.7, 127.4, 119.7, 115.9 (d, *J* = 19.0 Hz), 115.4, 113.8 (d, *J* = 6.3 Hz), 112.7 (d, *J* = 2.4 Hz), 83.5, 82.3; HRMS calcd for [C₁₆H₁₀FN₃O + H]⁺ 280.0881, found 280.0854.

4.1.2.3. 3-[(6-Ethynylquinazolin-4-yl)amino]-4-fluorophenol (14b). Yield: 38%; mp >350 °C (decomposed); ¹H NMR: δ 9.84 (s, 1H), 9.52 (s, 1H), 8.67 (s, 1H), 8.49 (s, 1H), 7.86 (d, *J* = 8.6 Hz, 1H), 7.75 (d, *J* = 8.6 Hz, 1H), 7.14–7.04 (m, 1H), 6.93–6.89 (m, 1H), 6.69–6.63 (m, 1H), 4.39 (s, 1H); ¹³C NMR: δ 158.1, 155.6, 153.4 (d, *J* = 1.7 Hz), 150.2 (d, *J* = 237.6 Hz), 149.4, 135.4, 128.2, 127.1, 126.0 (d, *J* = 13.9 Hz), 119.3, 116.1 (d, *J* = 21.5 Hz), 114.7, 114.2, 113.4 (d, *J* = 7.3 Hz), 82.9, 81.9; HRMS calcd for [C₁₆H₁₀FN₃O – H][–] 278.0735, found 278.0717.

4.1.2.4. 5-[(6-Ethynylquinazolin-4-yl)amino]-2,4-difluorophenol (14c). Yield: 38%; mp 286.2–287.6 °C; ¹H NMR: δ 9.98 (s, 1H), 9.84 (s, 1H), 8.65 (s, 1H), 8.49 (s, 1H), 7.87 (d, *J* = 8.5 Hz, 1H), 7.75 (d, *J* = 8.5 Hz, 1H), 7.32 (t, *J* = 10.5 Hz, 1H), 7.08 (t, *J* = 8.3 Hz, 1H), 4.41 (s, 1H); ¹³C NMR: δ 158.2, 155.6, 149.4, 149.1 (dd, *J* = 241.2, 10.8 Hz), 148.4 (dd, *J* = 242.9, 11.0 Hz), 141.0 (dd, *J* = 12.7, 2.7 Hz), 135.5, 128.2, 127.1, 121.5 (dd, *J* = 13.6, 3.4 Hz), 119.4, 116.2, 114.6, 104.8 (t, *J* = 24.4 Hz), 82.9, 81.9; HRMS calcd for [C₁₆H₉F₂N₃O – H][–] 296.0641, found 296.0673.

4.1.2.5. 3-[(6-Ethynylquinazolin-4-yl)amino]-2,6-difluorophenol (14d). Yield: 65%; mp 274.8–276.0 °C; ¹H NMR: δ 10.28 (s, 1H), 9.89 (s, 1H), 8.67 (s, 1H), 8.48 (s, 1H), 7.86 (d, *J* = 8.6 Hz, 1H), 7.75 (d, *J* = 8.6 Hz, 1H), 7.10–7.03 (m, 1H), 6.95–6.88 (m, 1H), 4.38 (s, 1H); ¹³C NMR: δ 158.8, 156.1, 151.1 (dd, *J* = 240.3, 5.4 Hz), 149.8, 148.4 (dd, *J* = 244.6, 6.6 Hz), 135.9, 134.7 (dd, *J* = 16.5, 15.4 Hz), 128.7, 127.5, 123.3 (dd, *J* = 10.9, 3.1 Hz), 119.8, 117.4 (d, *J* = 8.2 Hz), 115.0, 111.1 (dd, *J* = 19.4, 3.3 Hz), 83.4, 82.4; HRMS calcd for [C₁₆H₉F₂N₃O – H][–] 296.0641, found 296.0675.

4.1.3. 4-(3-Hydroxyanilino)-6-(1H-1,2,3-triazol-4-yl)quinazoline (9a)

A solution of **12** (149.7 mg, 0.5729 mmol, 1.0 equiv), trimethylsilyl azide (131.4 mg, 1.141 mmol, 2.0 equiv), and CuI (8.6 mg, 0.045 mmol, 0.079 equiv) in anhydrous DMF (0.90 mL) and MeOH (0.10 mL) was purged with nitrogen to remove oxygen. The reaction mixture was heated at 100 °C for 12 h. The solution was cooled to room temperature and diluted with water. The resulting solids were collected by filtration and re-dissolved in MeOH (5.0 mL). The solution was filtered, and the filtrate was concentrated under reduced pressure. The residue was purified by column chromatography to give **9a** (93.2 mg, 0.306 mmol) as yellow solids in 53% yield: mp 266.4–268.8 °C; ¹H NMR: δ 9.80 (s, 1H), 9.45 (brs, 1H), 9.00 (s, 1H), 8.56 (s, 1H), 8.43 (s, 1H), 8.30 (d, *J* = 8.6 Hz, 1H), 7.83 (d, *J* = 8.6 Hz, 1H), 7.39 (s, 1H), 7.24 (d, *J* = 8.0 Hz, 1H), 7.15 (t, *J* = 8.0 Hz, 1H), 6.54 (d, *J* = 8.0 Hz, 1H); ¹³C NMR: δ 158.2, 157.9, 155.0, 149.9, 146.3, 140.5, 130.9, 129.5, 128.9, 128.8, 120.0,

115.9, 113.7, 111.5, 110.1, 109.8; HRMS calcd for $[C_{16}H_{12}N_6O + H]^+$ 305.1145, found 305.1132.

4.1.4. Standard procedure for the synthesis of 4-(3-hydroxyanilino)-6-(1H-1,2,3-triazol-4-yl)quinazolines **9b–n**

Compound **12** or **14a–d** (~0.30 mmol, 1.0 equiv) and the corresponding alkyl azide (1.5 equiv) were added to a solution of $CuSO_4 \cdot H_2O$ (0.020 equiv), sodium ascorbate (0.010 equiv), and benzoic acid (0.20 equiv) in *t*-BuOH (2.0 mL) and water (1.0 mL). The reaction mixture was stirred at room temperature for 12 h. The solution was concentrated under reduced pressure to remove *t*-BuOH and then added with water (5.0 mL). The resulting precipitate was collected by filtration and purified by column chromatography to provide the targets **9b–n** in 27–95% yields.

4.1.4.1. 3-({6-[1-(2-Hydroxyethyl)-1H-1,2,3-triazol-4-yl]amino}phenol) (**9b**). Yield: 54%; mp 285.2–287.0 °C; 1H NMR: δ 9.86 (s, 1H), 9.44 (s, 1H), 9.05 (s, 1H), 8.64 (s, 1H), 8.56 (s, 1H), 8.32 (d, J = 8.7 Hz, 1H), 7.83 (d, J = 8.7 Hz, 1H), 7.41 (s, 1H), 7.26 (d, J = 8.0 Hz, 1H), 7.16 (t, J = 8.0 Hz, 1H), 6.55 (d, J = 8.0 Hz, 1H), 5.17 (t, J = 5.3 Hz, 1H), 4.50 (t, J = 5.2 Hz, 2H), 3.87–3.78 (m, 2H); ^{13}C NMR: δ 157.7, 157.3, 154.3, 149.2, 145.6, 140.0, 130.1, 128.9, 128.8, 128.4, 122.5, 118.9, 115.5, 113.2, 110.9, 109.6, 59.8, 52.5; HRMS calcd for $[C_{18}H_{16}N_6O_2 + H]^+$ 349.1408, found 349.1406.

4.1.4.2. 3-({6-[1-(3-Hydroxypropyl)-1H-1,2,3-triazol-4-yl]amino}phenol) (**9c**). Yield: 40%; mp 235.0–236.7 °C; 1H NMR: δ 9.83 (s, 1H), 9.45 (s, 1H), 9.01 (s, 1H), 8.62 (s, 1H), 8.55 (s, 1H), 8.27 (d, J = 8.6 Hz, 1H), 7.82 (d, J = 8.6 Hz, 1H), 7.39 (s, 1H), 7.24 (d, J = 7.8 Hz, 1H), 7.15 (t, J = 7.8 Hz, 1H), 6.53 (d, J = 7.8 Hz, 1H), 4.73 (s, 1H), 4.50 (t, J = 6.8 Hz, 2H), 3.43 (t, J = 6.8 Hz, 2H), 2.02 (p, J = 6.8 Hz, 2H); ^{13}C NMR: δ 157.7, 157.3, 154.4, 149.2, 145.7, 140.0, 130.2, 129.0, 128.7, 128.4, 122.0, 118.9, 115.4, 113.2, 110.9, 109.5, 57.3, 46.8, 32.8; HRMS calcd for $[C_{19}H_{18}N_6O_2 + H]^+$ 363.1564, found 363.1555.

4.1.4.3. 3-({6-[1-(2-Morpholinoethyl)-1H-1,2,3-triazol-4-yl]amino}phenol) (**9d**). Yield: 74%; mp 190.8–193.2 °C; 1H NMR: δ 9.86 (s, 1H), 9.44 (s, 1H), 9.02 (s, 1H), 8.62 (s, 1H), 8.56 (s, 1H), 8.26 (d, J = 8.6 Hz, 1H), 7.83 (d, J = 8.6 Hz, 1H), 7.39 (s, 1H), 7.24 (d, J = 8.0 Hz, 1H), 7.15 (t, J = 8.0 Hz, 1H), 6.53 (d, J = 8.0 Hz, 1H), 4.58 (t, J = 6.3 Hz, 2H), 3.54 (t, J = 4.0 Hz, 4H), 2.81 (t, J = 6.3 Hz, 2H), 2.44 (t, J = 4.0 Hz, 4H); ^{13}C NMR: δ 158.2, 157.8, 146.1, 140.5, 131.8, 130.8, 129.5, 129.4, 129.2, 122.7, 119.4, 113.7, 113.5, 111.4, 110.0, 109.8, 66.6, 57.9, 53.4, 47.3; HRMS calcd for $[C_{22}H_{23}N_7O_2 + H]^+$ 418.1986, found 418.1972.

4.1.4.4. 2-(4-{4-[(3-Hydroxyphenyl)amino]quinazolin-6-yl}-1H-1,2,3-triazol-1-yl)acetic acid (**9e**). Yield: 67%; mp 244.3–246.8 °C; 1H NMR: δ 9.88 (s, 1H), 9.42 (s, 1H), 9.06 (s, 1H), 8.61 (s, 1H), 8.31 (d, J = 7.2 Hz, 1H), 7.96–7.75 (m, 2H), 7.39 (s, 1H), 7.24 (d, J = 7.8 Hz, 1H), 7.16 (t, J = 7.8 Hz, 1H), 6.54 (d, J = 7.8 Hz, 1H), 5.39 (s, 2H); ^{13}C NMR: δ 158.1, 157.9, 154.6, 146.2, 140.4, 133.3, 130.7, 129.5, 129.2, 129.0, 123.9, 119.8, 113.8, 113.6, 111.6, 110.2, 110.0, 49.4; HRMS calcd for $[C_{19}H_{17}N_7O_2 + H]^+$ 376.1516, found 376.1537.

4.1.4.5. 2-(4-{4-[(3-Hydroxyphenyl)amino]quinazolin-6-yl}-1H-1,2,3-triazol-1-yl)acetamide (**9f**). Yield: 54%; mp 255.9–258.0 °C; 1H NMR: δ 9.90 (s, 1H), 9.42 (s, 1H), 8.58 (s, 1H), 8.44 (d, J = 6.8 Hz, 1H), 7.81 (d, J = 6.8 Hz, 1H), 7.45 (s, 1H), 7.39 (s, 1H), 7.24 (d, J = 7.8 Hz, 1H), 7.14 (t, J = 7.8 Hz, 1H), 6.55 (d, J = 7.8 Hz, 1H), 5.18 (s, 2H); ^{13}C NMR: δ 167.7, 160.2, 158.0, 157.3, 145.7, 139.9, 133.3, 130.4, 130.0, 129.7, 129.1, 124.3, 120.6, 114.2, 112.1, 112.0, 110.7, 52.2; HRMS calcd for $[C_{18}H_{14}N_6O_3 + H]^+$ 363.1200, found 363.1190.

4.1.4.6. 3-(4-{4-[(3-Hydroxyphenyl)amino]quinazolin-6-yl}-1H-1,2,3-triazol-1-yl)propanoic acid (**9g**). Yield: 50%; mp 266.7–268.1 °C; 1H NMR: δ 12.50 (s, 1H), 9.83 (s, 1H), 9.42 (s, 1H), 9.02 (s, 1H), 8.61 (s, 1H), 8.28 (s, 1H), 7.84 (brs, 1H), 7.39 (s, 1H), 7.24 (d, J = 7.8 Hz, 1H), 7.16 (t, J = 7.8 Hz, 1H), 6.54 (d, J = 7.8 Hz, 1H), 4.66 (brs, 2H), 2.98 (brs, 2H); ^{13}C NMR: δ 158.0, 157.9, 146.1, 140.5, 140.2, 130.6, 129.5, 129.2, 122.7, 119.6, 118.2, 113.7, 113.5, 111.7, 111.5, 110.1, 109.9, 46.3, 29.5; HRMS calcd for $[C_{19}H_{16}N_6O_3 + H]^+$ 377.1357, found 377.1377.

4.1.4.7. 3-(4-{4-[(3-Hydroxyphenyl)amino]quinazolin-6-yl}-1H-1,2,3-triazol-1-yl)propanamide (**9h**). Yield: 95%; mp 208.8–210.2 °C; 1H NMR: δ 9.82 (s, 1H), 9.42 (s, 1H), 8.98 (s, 1H), 8.55 (s, 1H), 8.54 (s, 1H), 8.27 (d, J = 8.7 Hz, 1H), 7.82 (d, J = 8.7 Hz, 1H), 7.45 (s, 1H), 7.38 (t, J = 2.1 Hz, 1H), 7.23 (d, J = 7.6 Hz, 1H), 7.15 (t, J = 7.6 Hz, 1H), 6.95 (s, 1H), 6.53 (dd, J = 7.6, 2.1 Hz, 1H), 4.63 (t, J = 6.6 Hz, 2H), 2.76 (t, J = 6.6 Hz, 2H); ^{13}C NMR: δ 171.5, 158.1, 157.8, 154.8, 146.0, 141.7, 140.5, 130.6, 129.6, 129.5, 129.2, 129.1, 122.8, 119.5, 113.7, 111.5, 110.1, 46.5, 35.6; HRMS calcd for $[C_{19}H_{17}N_7O_2 + H]^+$ 376.1516, found 376.1537.

4.1.4.8. 3-(4-{4-[(3-Hydroxyphenyl)amino]quinazolin-6-yl}-1H-1,2,3-triazol-1-yl)-*N*-methylpropanamide (**9i**). Yield: 55%; mp 121.5–124.0 °C; 1H NMR: δ 9.84 (s, 1H), 9.44 (s, 1H), 9.00 (s, 1H), 8.60 (brs, 1H), 8.54 (s, 1H), 8.27 (d, J = 6.1 Hz, 1H), 7.94 (d, J = 6.1 Hz, 1H), 7.80 (brs, 1H), 7.38 (s, 1H), 7.23 (d, J = 8.0 Hz, 1H), 7.15 (t, J = 8.0 Hz, 1H), 6.54 (d, J = 8.0 Hz, 1H), 4.65 (t, J = 6.6 Hz, 2H), 2.76 (t, J = 6.6 Hz, 2H), 2.54 (d, J = 4.6 Hz, 3H); ^{13}C NMR: δ 169.9, 158.1, 157.8, 146.0, 140.5, 130.6, 129.5, 129.2, 125.8, 122.8, 119.5, 116.2, 113.8, 113.6, 111.5, 110.2, 110.0, 46.6, 35.8, 26.0; HRMS calcd for $[C_{20}H_{19}N_7O_2 + H]^+$ 390.1673, found 390.1650.

4.1.4.9. 3-(4-{4-[(3-Hydroxyphenyl)amino]quinazolin-6-yl}-1H-1,2,3-triazol-1-yl)-*N,N*-dimethylpropanamide (**9j**). Yield: 45%; mp 241.9–243.1 °C; 1H NMR: δ 9.85 (s, 1H), 9.45 (brs, 1H), 9.06 (s, 1H), 8.61 (s, 1H), 8.55 (s, 1H), 8.28 (d, J = 8.7 Hz, 1H), 7.82 (d, J = 8.7 Hz, 1H), 7.38 (s, 1H), 7.23 (d, J = 8.4 Hz, 1H), 7.15 (t, J = 8.4 Hz, 1H), 6.53 (d, J = 8.4 Hz, 1H), 4.64 (t, J = 6.6 Hz, 2H), 3.03 (t, J = 6.6 Hz, 2H), 2.94 (s, 3H), 2.81 (s, 3H); ^{13}C NMR: δ 169.6, 158.2, 157.8, 154.9, 149.7, 146.0, 140.5, 130.6, 129.5, 129.2, 128.9, 123.0, 119.4, 116.0, 113.7, 111.4, 110.1, 46.4, 36.9, 35.3, 33.3; HRMS calcd for $[C_{21}H_{21}N_7O_2 + H]^+$ 404.1829, found 404.1844.

4.1.4.10. 3-(4-{4-[(4-Fluoro-3-hydroxyphenyl)amino]quinazolin-6-yl}-1H-1,2,3-triazol-1-yl)propanamide (**9k**). Yield: 30%; mp 274.8–276.0 °C; 1H NMR: δ 10.03 (s, 1H), 9.99 (s, 1H), 9.16 (s, 1H), 8.75 (s, 1H), 8.54 (s, 1H), 8.31 (d, J = 8.7 Hz, 1H), 7.82 (d, J = 8.7 Hz, 1H), 7.64 (dd, J = 8.2, 2.4 Hz, 1H), 7.58 (s, 1H), 7.32–7.23 (m, 1H), 7.12 (dd, J = 11.0, 8.9 Hz, 1H), 6.98 (s, 1H), 4.65 (t, J = 6.6 Hz, 2H), 2.80 (t, J = 6.6 Hz, 2H); ^{13}C NMR: δ 171.1, 157.8, 154.4, 149.2, 147.7 (d, J = 237.8 Hz), 145.7, 144.4 (d, J = 12.8 Hz), 135.4 (d, J = 2.4 Hz), 130.0, 128.7, 128.4, 122.5, 119.4, 115.5 (d, J = 1.4 Hz), 115.3, 113.7 (d, J = 6.2 Hz), 112.6 (d, J = 2.1 Hz), 46.1, 35.2; HRMS calcd for $[C_{19}H_{16}FN_7O_2 + H]^+$ 394.1422, found 394.1410.

4.1.4.11. 3-(4-{4-[(2-Fluoro-5-hydroxyphenyl)amino]quinazolin-6-yl}-1H-1,2,3-triazol-1-yl)propanamide (**9l**). Yield: 27%; mp 285.5–287.0 °C; 1H NMR: δ 9.88 (s, 1H), 9.49 (s, 1H), 8.95 (s, 1H), 8.54 (s, 1H), 8.48 (s, 1H), 8.31 (d, J = 8.7 Hz, 1H), 7.84 (d, J = 8.7 Hz, 1H), 7.48 (s, 1H), 7.10 (t, J = 9.5 Hz, 1H), 7.00–6.94 (m, 2H), 6.69–6.63 (m, 1H), 4.66 (t, J = 6.5 Hz, 2H), 2.78 (t, J = 6.5 Hz, 2H); ^{13}C NMR: δ 171.0, 158.6, 154.7, 153.4 (d, J = 1.6 Hz), 150.2 (d, J = 237.2 Hz), 149.2, 145.5, 130.3, 128.7, 128.4, 126.4 (d, J = 13.8 Hz), 122.3, 119.0, 116.0 (d, J = 21.6 Hz), 115.1, 114.3, 113.2 (d, J = 7.3 Hz), 46.1, 35.2; HRMS calcd for $[C_{19}H_{16}FN_7O_2 + H]^+$ 394.1422, found 394.1403.

4.1.4.12. 3-(4-{4-[(2,4-Difluoro-5-hydroxyphenyl)amino]quinazolin-6-yl}-1H-1,2,3-triazol-1-yl)propanamide (**9m**). Yield: 42%; mp 298.7–300.3 °C; ¹H NMR: δ 10.05 (brs, 1H), 9.99 (s, 1H), 9.02 (s, 1H), 8.60 (s, 1H), 8.46 (s, 1H), 8.31 (d, *J* = 8.7 Hz, 1H), 7.83 (d, *J* = 8.7 Hz, 1H), 7.52 (s, 1H), 7.29 (t, *J* = 10.6 Hz, 1H), 7.15 (t, *J* = 8.3 Hz, 1H), 6.97 (s, 1H), 4.65 (t, *J* = 6.6 Hz, 2H), 2.78 (t, *J* = 6.6 Hz, 2H); ¹³C NMR: δ 171.0, 158.7, 154.7, 149.2, 149.1 (dd, *J* = 240.5, 10.4 Hz), 148.3 (dd, *J* = 242.5, 11.1 Hz), 145.5, 141.1 (dd, *J* = 12.6, 2.7 Hz), 130.2, 128.7, 128.4, 122.3, 121.8 (dd, *J* = 13.6, 3.6 Hz), 119.2, 116.3, 115.0, 104.7 (t, *J* = 24.3 Hz), 46.1, 35.2; HRMS calcd for [C₁₉H₁₅F₂N₇O₂ + H]⁺ 412.1328, found 412.1350.

4.1.4.13. 3-(4-{4-[(2,4-Difluoro-3-hydroxyphenyl)amino]quinazolin-6-yl}-1H-1,2,3-triazol-1-yl)propanamide (**9n**). Yield: 34%; mp 248.1–249.9 °C; ¹H NMR: δ 10.29 (brs, 1H), 10.04 (s, 1H), 9.02 (s, 1H), 8.59 (s, 1H), 8.45 (s, 1H), 8.31 (d, *J* = 8.7 Hz, 1H), 7.84 (d, *J* = 8.7 Hz, 1H), 7.52 (s, 1H), 7.07 (t, *J* = 9.6 Hz, 1H), 7.02–6.86 (m, 2H), 4.65 (t, *J* = 6.6 Hz, 2H), 2.78 (t, *J* = 6.6 Hz, 2H); ¹³C NMR: δ 171.0, 158.8, 154.7, 150.6 (dd, *J* = 240.2, 5.1 Hz), 149.2, 148.1 (dd, *J* = 244.4, 6.6 Hz), 145.5, 134.3 (t, *J* = 15.7 Hz), 130.2, 128.7, 128.4, 123.1 (dd, *J* = 10.9, 2.9 Hz), 122.3, 119.2, 116.9 (d, *J* = 7.9 Hz), 115.0, 110.6 (dd, *J* = 19.5, 2.8 Hz), 46.1, 35.2; HRMS calcd for [C₁₉H₁₅F₂N₇O₂ + H]⁺ 412.1328, found 412.1344.

4.2. Kinase assays

The kinase inhibitory activity of **9a–n** and reference standards (**1**, **4**, and **6**) was determined on the radiometric assays by measuring the amount of ³³P incorporated into the substrate in the presence of a compound. For Raf kinase assays, a reaction mixture (25 μL, final volume) containing recombinant B-Raf (5 ng, Upstate) or recombinant B-Raf^{V600E} (5 ng, Upstate) or recombinant C-Raf (2 ng, Upstate) with 500 ng MEK1^{K97R} (Millipore), 50 mM Tris/HCl (pH 7.5), 1 mM EGTA, 1 mM Na₃VO₄, 1% 2-mercaptoethanol, 0.1% Brij 35 (Millipore), 0.2 mg/mL BSA (Sigma), 8 μM ATP (Sigma), 0.5 μCi [³³P]ATP (specific activity 3000 Ci/mmol, PerkinElmer), and a compound (or 4% DMSO) was incubated at 30 °C. After 30 min, the reaction was stopped by adding 3% phosphoric acid. The solution was subsequently harvested onto a 96-well GF/B UniFilter (PerkinElmer), and the radioactivity of the filter was counted on a TopCount microplate scintillation counter (PerkinElmer). The compounds were 3-fold serially diluted in triplication for the assays. Software GraphPad Prism 4 (GraphPad Software Inc.) was used to analyze the results.

For EGFR assays, a reaction mixture (25 μL, final volume) of kinase domain of EGFR (25 ng, Millipore) or EGFR^{T790M} (25 ng, Millipore) with 5 μg poly(Glu-Tyr) (Sigma), 10 mM MOPS (pH 7.0), 0.3 mM EDTA, 0.5% glycerol, 0.001% Brij-35 (Sigma), 10 mM MnCl₂, 0.1 mg/mL BSA (Sigma), 100 μM ATP (Sigma), 0.1 μCi [³³P]ATP (specific activity 3000 Ci/mmol, PerkinElmer), and a compound (or 4% DMSO) was incubated at 30 °C. For EGFR assay, the incubation time was 30 min. For EGFR^{T790M} assay, the incubation time was 60 min. The reaction was stopped, processed, and analyzed following the same procedures for the Raf kinase assays. For VEGFR2 and PDGFR-β kinase assays, the compounds were assayed following our published methods [53].

4.3. In vitro antiproliferative assays

The potency of the compounds to inhibit the proliferation of A375 (ATCC CRL-1619), PC-9 (ECACC 90071810), HCC827 (ATCC CRL-2868), and H1975 (ATCC CRL-5908) cancer cells was determined using the CellTiter96 assay kit (Promega) as previously described [54]. The cell density for A375, PC-9, and H1975 cells was 2,000/well for the assay. For HCC827 cells, the cell density was 8,000/well. The GI₅₀ values presented in Tables 3 were averaged from three independent dose–response curves.

4.4. Computational method

The crystal structures of B-Raf, B-Raf^{V600E}, and VEGFR2 were retrieved from Protein Data Bank. The entries of these crystal structures are shown in Fig. 3 and Table 4. The structures of **9m** and drug **3** were constructed by Chemdraw and optimized by the MM2 method in Chem3D. The macromolecules were processed by removal of the co-crystallized ligand and waters, addition of hydrogens, and assignment of Gasteiger–Marsili charges using AutoDockTools 1.5.6. For the ligands, the root of torsion trees and the active torsions were generated automatically. The grid box size was set to 60 × 60 × 60 (spacing 0.375 Å) and centered at the cavity of the removed ligand. The grid map was calculated by Autogrid. Docking was performed using Autodock 4.2.6 with the default parameters. The interaction of **9m** with 1UWH (B-Raf), 1UWJ (B-Raf^{V600E}), and 4AGD (VEGFR2) was analyzed by Discovery Studio Visualizer (BIOVIA software, Inc.) and are shown in Fig. 3. The calculated binding energy of the most stable poses of **9m** in the kinases was retrieved from the docking results and shown in Table 4.

Author contribution

C.-I.L. designed the compounds and revised the manuscript; C.-B.L. designed the biological study and analyzed the biological data; C.-S.C., F.-Y.C., Y.-H.C., Y.-C.W., W.-Y.H., T.-H.L., G.-R.H., H.-Y.H., and C.-S.T. synthesized the compounds; S.-Y.C. screened the compounds and performed the biological study; Y.-J.L. analyzed the spectroscopic data; S.-H.C. and J.-J.H. designed the compounds and performed the docking simulations; J.-J.H. prepared the manuscript.

Funding sources

This research was supported by the Ministry of Science and Technology of the Republic of China (Taiwan, MOST 102–2113-M–415–005–MY2).

Declaration of Competing Interest

The authors declare that they have no known competing financial interests or personal relationships that could have appeared to influence the work reported in this paper.

Acknowledgements

We thank Prof. Cheng-Liang Huang for helpful discussions.

Appendix A. Supplementary data

Supplementary data to this article can be found online at <https://doi.org/10.1016/j.bioorg.2021.104715>.

References

- [1] P. Blume-Jensen, T. Hunter, Oncogenic kinase signaling, *Nature* 411 (2001) 355–365.
- [2] P.A. Schwartz, B.W. Murray, Protein kinase biochemistry and drug discovery, *Bioorg. Chem.* 39 (2011) 192–210.
- [3] K.S. Bhullar, N.O. Lagarón, E.M. McGowan, I. Parmar, A. Jha, B.P. Hubbard, H.P. V. Rupasinghe, Kinase-targeted cancer therapies: progress, challenges and future directions, *Mol. Cancer* 17 (2018) 48.
- [4] R. Roskoski Jr., Properties of FDA-approved small molecule protein kinase inhibitors, *Pharmacol. Res.* 144 (2019) 19–50.
- [5] F. Giardiello, G. Tortora, EGFR antagonists in cancer treatment, *N. Engl. J. Med.* 358 (2008) 1160–1174.
- [6] S.P. Ivy, J.Y. Wick, B.M. Kaufman, An overview of small-molecule inhibitors of VEGFR signaling, *Nat. Rev. Clin. Oncol.* 6 (2009) 569–579.
- [7] R. Rosell, T. Moran, C. Queralt, R. Porta, F. Cardenal, C. Camps, M. Majem, G. Lopez-Vivanco, D. Isla, M. Provencio, A. Insa, B. Massuti, J.L. Gonzalez-Larriba, L. Paz-Ares, I. Bover, R. Garcia-Campelo, M.A. Moreno, S. Catot, C. Rolfó, N. Reguart, R. Palmero, J.M. Sánchez, R. Bastus, C. Mayo, J. Bertran-Alamillo, M.

- A. Molina, J.J. Sanchez, M. Taron, Screening for epidermal growth factor receptor mutations in lung cancer, *N. Engl. J. Med.* 361 (2009) 958–967.
- [8] H.F. Dvorak, Vascular permeability factor/vascular endothelial growth factor: A critical cytokine in tumor angiogenesis and a potential target for diagnosis and therapy, *J. Clin. Oncol.* 20 (2002) 4368–4380.
- [9] Y. Takahashi, Y. Kitadai, C.D. Bucana, K.R. Cleary, L.M. Ellis, Expression of vascular endothelial growth factor and its receptor, KDR, correlates with vascularity, metastasis, and proliferation of human colon cancer, *Cancer Res.* 55 (1995) 3964–3968.
- [10] R.-T.-P. Poon, S.-T. Fan, J. Wong, Clinical implications of circulating angiogenic factors in cancer patients, *J. Clin. Oncol.* 19 (2001) 1207–1225.
- [11] C.G. Azzoli, S. Baker Jr., S. Temin, W. Pao, T. Aliff, J. Brahmer, D.H. Johnson, J. Laskin, G. Masters, D. Milton, L. Nordquist, D.G. Pfister, S. Piantadosi, J. H. Schiller, R. Smith, T.J. Smith, J.R. Strawn, D. Trent, G. Giaccone, American Society of Clinical Oncology Clinical Practice Guideline update on chemotherapy for stage IV non-small-cell lung cancer, *J. Clin. Oncol.* 27 (2009) 6251–6266.
- [12] L. Huang, Z. Huang, Z. Bai, R. Xie, L. Sun, K. Lin, Development and strategies of VEGFR-2/KDR Inhibitors, *Future Med. Chem.* 4 (2012) 1839–1852.
- [13] H. Jin, H.-G. Dan, C.-W. Rao, Research progress in quinazoline derivatives as multi-target tyrosine kinase inhibitors, *Heterocycl. Commun.* 24 (2018) 1–10.
- [14] A. Ayati, S. Moghimi, S. Salarinejad, M. Safavi, B. Pouramiri, A. Foroumadi, A review on progression of epidermal growth factor receptor (EGFR) inhibitors as an efficient approach in cancer targeted therapy, *Bioorg. Chem.* 99 (2020), 103811.
- [15] G. Blackledge, S. Averbuch, Gefitinib ('Iressa', ZD1839) and new epidermal growth factor receptor inhibitors, *Br. J. Cancer* 90 (2004) 566–572.
- [16] S. Dhillon, A.J. Wagstaff, Lapatinib, *Drugs* 67 (2007) 2101–2108.
- [17] P.B. Langmuir, A. Yver, Vandetanib for the treatment of thyroid cancer, *Clin. Pharmacol. Ther.* 91 (2012) 71–80.
- [18] H.A. Allam, E.E. Aly, A.K.B.A.W. Farouk, A.M. El Kerdawy, E. Rashwan, S.E. S. Abbass, Design and Synthesis of some new 2,4,6-trisubstituted quinazoline EGFR inhibitors as targeted anticancer agents, *Bioorg. Chem.* 98 (2020), 103726.
- [19] S.R.A. El Hadi, D.S. Lasheen, D.H. Soliman, E.Z. Elrazaz, K.A.M. Abouzid, Scaffold hopping and redesign approaches for quinazoline based urea derivatives as potent VEGFR-2 inhibitors, *Bioorg. Chem.* 101 (2020), 103961.
- [20] S.-Y. Lin, C.-F. Chang, M.S. Coumar, P.-Y. Chen, F.-M. Kuo, C.-H. Chen, M.-C. Li, W.-H. Lin, P.-C. Kuo, S.-Y. Wang, A.-S. Li, C.-Y. Lin, C.-M. Yang, T.-K. Yeh, J.-S. Song, J.T.A. Hsu, H.-P. Hsieh, Drug-like property optimization: Discovery of orally bioavailable quinazoline-based multi-targeted kinase inhibitors, *Bioorg. Chem.* 98 (2020), 103680.
- [21] C. Wellbrock, M. Karasarides, R. Marais, The RAF proteins take centre stage, *Nat. Rev. Mol. Cell Biol.* 5 (2004) 875–885.
- [22] C. Peyssonnaud, A. Eychène, The Raf/MEK/ERK pathway: new concepts of activation, *Biol. Cell* 93 (2001) 53–62.
- [23] H. Davies, G.R. Bignell, C. Cox, P. Stephens, S. Edkins, S. Clegg, J. Teague, H. Woffendin, M.J. Garnett, W. Bottomley, N. Davis, E. Dicks, R. Ewing, Y. Floyd, K. Gray, S. Hall, R. Hawes, J. Hughes, V. Kosmidou, A. Menzies, C. Mould, A. Parker, C. Stevens, S. Watt, S. Hooper, R. Wilson, H. Jayatilake, B.A. Gusterson, C. Cooper, J. Shipley, D. Hargrave, K. Pritchard-Jones, N. Maitland, G. Chenevix-Trench, G.J. Riggins, D.D. Bigner, G. Palmieri, A. Cossu, A. Flanagan, A. Nicholson, J.W.C. Ho, S.Y. Leung, S.T. Yuen, B.L. Weber, H.F. Seigler, T.L. Darrow, H. Paterson, R. Marais, C.J. Marshall, R. Wooster, M.R. Stratton, P.A. Futreal, Mutations of the BRAF gene in human cancer, *Nature* 417 (2002) 949–954.
- [24] C. Michalogioli, L.C.W. Vredevelde, W.J. Mooi, D.S. Peepker, BRAF(E600) in benign and malignant human tumours, *Oncogene* 27 (2008) 877–895.
- [25] Y. Cohen, M. Xing, E. Mambo, Z. Guo, G. Wu, B. Trink, U. Beller, W.H. Westra, P. W. Ladenson, D. Sidransky, BRAF mutation in papillary thyroid carcinoma, *J. Natl. Cancer Inst.* 95 (2003) 625–627.
- [26] X. Xu, R.M. Quiros, P. Gattuso, K.B. Ain, R.A. Prinz, High prevalence of BRAF gene mutation in papillary thyroid carcinomas and thyroid tumor cell lines, *Cancer Res.* 63 (2003) 4561–4567.
- [27] A.A. Samatar, P.I. Poulikakos, Targeting RAS-ERK signalling in cancer: promises and challenges, *Nat. Rev. Drug Discov.* 13 (2014) 928–942.
- [28] G. Bollag, J. Tsai, J. Zhang, C. Zhang, P. Ibrahim, K. Nolop, P. Hirth, Vemurafenib: the first drug approved for BRAF-mutant cancer, *Nat. Rev. Drug Discov.* 11 (2012) 873–886.
- [29] L. Khoja, D. Hogg, Dabrafenib in the treatment of metastatic or unresectable melanoma, *Expert Rev. Anticancer Ther.* 15 (2015) 265–276.
- [30] J. Downward, Targeting Ras signalling pathways in cancer therapy, *Nat. Rev. Cancer* 3 (2003) 11–22.
- [31] B. Escudier, T. Eisen, W.M. Stadler, C. Szczylik, S. Oudard, M. Siebels, S. Negrier, C. Chèvre, E. Solska, A.A. Desai, F. Rolland, T. Demkow, T.E. Hutson, M. Gore, S. Freeman, B. Schwartz, M. Shan, R. Simantov, R.M. Bukowski, TARGET Study Group Sorafenib in advanced clear-cell renal-cell carcinoma, *N. Engl. J. Med.* 356 (2007) 125–134.
- [32] J.M. Llovet, S. Ricci, V. Mazzaferro, P. Hilgard, E. Gane, J.-F. Blanc, A.C. de Oliveira, A. Santoro, J.-L. Raouf, A. Forner, M. Schwartz, C. Porta, S. Zeuzem, L. Bolondi, T.F. Greten, P.R. Galle, J.-F. Seitz, I. Borbath, D. Häussinger, T. Giannaris, M. Shan, M. Moscovici, D. Voliotis, J. Bruix, Sorafenib in advanced hepatocellular carcinoma, *N. Engl. J. Med.* 358 (2008) 378–390.
- [33] L. Thomas, S.Y. Lai, W. Dong, L. Feng, R. Dadu, R.M. Regone, M.E. Cabanillas, Sorafenib in metastatic thyroid cancer: a systematic review, *Oncologist* 19 (2014) 251–258.
- [34] R.B. Corcoran, H. Ebi, A.B. Turke, E.M. Coffee, M. Nishino, A.P. Cogdill, R. D. Brown, P. Della Pelle, D. Dias-Santagata, K.E. Hung, K.T. Flaherty, A. Piris, J. A. Wargo, J. Settleman, M. Mino-Kenudson, J.A. Engelman, EGFR-mediated re-activation of MAPK signaling contributes to insensitivity of BRAF mutant colorectal cancers to RAF inhibition with vemurafenib, *Cancer Discov.* 2 (2012) 227–235.
- [35] A. Prabhalla, C. Sun, S. Huang, F. Di Nicolantonio, R. Salazar, D. Zecchin, R. L. Bejersbergen, A. Bardelli, R. Bernards, Unresponsiveness of colon cancer to BRAF(V600E) inhibition through feedback activation of EGFR, *Nature* 483 (2012) 100–103.
- [36] Q. Wang, W.-g. Hu, Q.-b. Song, J. Wei, BRAF V600E mutation as a predictive factor of anti-EGFR monoclonal antibodies therapeutic effects in metastatic colorectal cancer: a meta-analysis, *Chin. Med. Sci. J.* 29 (2014) 197–203.
- [37] S. Caporali, A. Amaro, L. Levati, E. Alvino, P.M. Lical, S. Mastroeni, F. Ruffini, L. Bonmassar, G.C. Antonini Cappellini, N. Felli, A. Carè, U. Pfeffer, S. D'Atri, miR-126-3p down-regulation contributes to dabrafenib acquired resistance in melanoma by up-regulating ADAM9 and VEGF-A, *J. Exp. Clin. Cancer Res.* 38 (2019) 272.
- [38] K. Connolly, D. Brungs, E. Szeto, R.J. Epstein, Anticancer activity of combination targeted therapy using cetuximab plus vemurafenib for refractory BRAF^{V600E}-mutant metastatic colorectal carcinoma, *Curr. Oncol.* 21 (2014) e151–e154.
- [39] V. Comunanza, D. Corà, F. Orso, F.M. Consonni, E. Middonti, F. Di Nicolantonio, A. Buzdin, A. Sica, E. Medico, D. Sngiolo, D. Taverna, F. Bussolino, VEGF blockade enhances the antitumor effect of BRAF^{V600E} inhibition, *EMBO Mol. Med.* 9 (2017) 219–237.
- [40] H. Cheng, Y. Chang, L. Zhang, J. Luo, Z. Tu, X. Lu, Q. Zhang, J. Lu, X. Ren, K. Ding, Identification and optimization of new dual inhibitors of B-Raf and epidermal growth factor receptor kinases for overcoming resistance against vemurafenib, *J. Med. Chem.* 57 (2014) 2692–2703.
- [41] O. McDonald, K. Lackey, R. Davis-Ward, E. Wood, V. Samano, P. Maloney, F. Deanda, R. Hunter, Aza-stilbenes as potent and selective c-RAF inhibitors, *Bioorg. Med. Chem. Lett.* 16 (2006) 5378–5383.
- [42] D. Kitagawa, K. Yokota, M. Gouda, Y. Narumi, H. Ohmoto, E. Nishiwaki, K. Akita, Y. Kirii, Activity-based kinase profiling of approved tyrosine kinase inhibitors, *Genes Cells* 18 (2013) 110–122.
- [43] J.-J. Huang, C.-B. Liao, P.-N. Chen, Quinazoline compounds as kinase inhibitors, *US Patent* 8785459 (2014).
- [44] T. Jin, S. Kamijo, Y. Yamamoto, Copper-catalyzed synthesis of *N*-unsubstituted 1,2,3-triazoles from nonactivated terminal alkynes, *Eur. J. Org. Chem.* 3789–3791 (2004).
- [45] S.M. Wilhelm, C. Carter, L. Tang, D. Wilkie, A. McNabola, H. Rong, C. Chen, X. Zhang, P. Vincent, M. McHugh, Y. Cao, J. Shujath, S. Gawlak, D. Eveleigh, B. Rowley, L. Liu, L. Adnane, M. Lynch, D. Auclair, I. Taylor, R. Gedrich, A. Voznesensky, B. Riedl, L.E. Post, G. Bollag, P.A. Trail, BAY 43-9006 exhibits broad spectrum oral antitumor activity and targets the RAF/MEK/ERK pathway and receptor tyrosine kinases involved in tumor progression and angiogenesis, *Cancer Res.* 64 (2004) 7099–7109.
- [46] G. Bollag, P. Hirth, J. Tsai, J. Zhang, P.N. Ibrahim, H. Cho, W. Spevak, C. Zhang, Y. Zhang, G. Habets, E.A. Burton, B. Wong, G. Tsang, B.L. West, B. Powell, R. Shellooe, A. Marimuthu, H. Nguyen, K.Y.J. Zhang, D.R. Artis, J. Schlessinger, F. Su, B. Higgins, R. Iyer, K. D'Andrea, A. Koehler, M. Stumm, P.S. Lin, R.J. Lee, J. Grippo, I. Puzanov, K.B. Kim, A. Ribas, G.A. McArthur, J.A. Sosman, P. B. Chapman, K.T. Flaherty, X. Xu, K.L. Nathanson, K. Nolop, Clinical efficacy of a RAF inhibitor needs broad target blockade in BRAF-mutant melanoma, *Nature* 467 (2010) 596–599.
- [47] (a) B. Agianian, E. Gavathiotis, Current insights of BRAF inhibitors in cancer, *J. Med. Chem.* 61 (2018) 5775–5793; (b) U.M. Ammar, M.S. Abdel-Maksoud, C.-H. Oh, Recent advances of RAF (rapidly accelerated fibrosarcoma) inhibitors as anti-cancer agents, *Eur. J. Med. Chem.* 158 (2018) 144–166.
- [48] Q. Zhang, Y. Diao, F. Wang, Y. Fu, F. Tang, Q. You, H. Zhou, Design and discovery of 4-anilinoquinazoline ureas as multikinase inhibitors targeting BRAF, VEGFR-2 and EGFR, *Med. Chem. Commun.* 4 (2013) 979–986.
- [49] G. Hatzivassiliou, K. Song, I. Yen, B.J. Brandhuber, D.J. Anderson, R. Alvarado, M. J.C. Ludlam, D. Stokoe, S.L. Gloor, G. Vigers, T. Morales, I. Aliagas, B. Liu, S. Sideris, K.P. Hoeflich, B.S. Jaiswal, S. Seshagiri, H. Koepfen, M. Belvin, L. S. Friedman, S. Malek, RAF inhibitors prime wild-type RAF to activate the MAPK pathway and enhance growth, *Nature* 464 (2010) 431–435.
- [50] P.T.C. Wan, M.J. Garnett, S.M. Roe, S. Lee, D. Niculescu-Duvaz, V.M. Good, C. M. Jones, C.J. Marshall, C.J. Springer, D. Barford, R. Marais, Cancer Genome Project, Mechanism of activation of the RAF-ERK signaling pathway by oncogenic mutations of B-RAF, *Cell* 116 (2004) 855–867.
- [51] G.M. Morris, R. Huey, W. Lindstrom, M.F. Sanner, R.K. Belew, D.S. Goodsell, A. J. Olson, AutoDock4 and AutoDockTools4: Automated docking with selective receptor flexibility, *J. Comput. Chem.* 30 (2009) 2785–2791.
- [52] M. McTigue, B.W. Murray, J.H. Chen, Y.-L. Deng, J. Solowiej, R.S. Kania, Molecular conformations, interactions, and properties associated with drug efficiency and clinical performance among VEGFR TK inhibitors, *Proc. Natl. Acad. Sci. U.S.A.* 109 (2012) 18281–18289.
- [53] J.-J. Huang, Y.-H. Lin, C.-L. Lai, S.-C. Yang, S.F. Lin, J.-Y. Yang, H.-H. Huang, C. Liu, W.-Y. Wei, S.-H. Chuang, C.-C. Chiang, Y.-S.E. Lee, C.-B. Liao, C.Y. Chern, The inhibition profiles of 4'-acylpyrrole-5-fluorindolin-2-ones with a C-3' side chain for VEGFR2, PDGFR- β , and FGFR-1 protein kinases, *J. Chin. Chem. Soc.* 67 (2020) 422–429.
- [54] C.-C. Chiang, Y.-H. Lin, S.F. Lin, C.-L. Lai, C. Liu, W.-Y. Wei, S.-C. Yang, R.-W. Wang, L.-W. Teng, S.H. Chuang, J.-M. Chang, T.-T. Yuan, Y.-S. Lee, P. Chen, W.-K. Chi, J.-Y. Yang, H.-J. Huang, C.-B. Liao, J.-J. Huang, Discovery of pyrrole-indoline-2-ones as Aurora kinase inhibitors with a different inhibition profile, *J. Med. Chem.* 53 (2010) 5929–5941.